Cenozoic vertical motions of the Catalan coastal ranges (NE Spain): the role of tectonics, isostasy and surface transport.

Gaspar Escribano, J.M.; Garcia-Castellanos, D.; Roca, E.; Cloetingh, S.A.P.L.

published in
Tectonics
2004

DOI (link to publisher)
10.1029/2003TC001511

Cenozoic vertical motions of the Catalan Coastal Ranges (NE Spain): The role of tectonics, isostasy, and surface transport

J. M. Gaspar-Escribano[1] and D. Garcia-Castellanos

Faculty of Earth and Life Sciences, Vrije Universiteit, Amsterdam, Netherlands

E. Roca

Facultat de Geologia, Universitat de Barcelona, Barcelona, Spain

S. Cloetingh

Faculty of Earth and Life Sciences, Vrije Universiteit, Amsterdam, Netherlands

Received 13 February 2003; revised 8 September 2003; accepted 6 October 2003; published 17 January 2004.

[1] We analyze the Cenozoic topographic evolution of the Catalan Coastal Ranges (NE Spain) and the role of fault activity, erosion, sedimentation, and isostasy in controlling uplift and subsidence. A forward numerical model constrained by an extensive geological and geophysical data set is used to examine the temporal and spatial record of Cenozoic vertical motions. We show that the effect of isostasy, erosion, and sedimentation is as important as the contribution of fault deformation to the topography of the Catalan Coastal Ranges. The model predicts that Paleogene topography generation by thrusting was compensated by erosion (up to 1.3 km) and isostatic subsidence (up to 1.2 km), resulting in a 1.2–1.9 km high mountain range by the end of compression (29 Ma). During the Neogene, strong tectonic subsidence related to normal faulting and the consequent flexural uplift (of 0.7–1.2 km), surface erosion (as much as 1.6–2.3 km), and sedimentation (up to 4.5 km) led to the present landscape configuration. Extension rates along the Barcelona fault controlled flexural uplift and, in combination with erosion and sedimentation processes, led to the migration of the topographic maximum of the Prelitoral Range toward the easternmost Ebro Basin. *INDEX TERMS:* 8105 Tectonophysics: Continental margins and sedimentary basins (1212); 8015 Structural Geology: Local crustal structure; 3210 Mathematical Geophysics: Modeling; 8109 Tectonophysics: Continental tectonics—extensional (0905); *KEYWORDS:* modeling, vertical motions, NE Spain. **Citation:** Gaspar-Escribano, J. M., D. Garcia-Castellanos, E. Roca, and S. Cloetingh (2004), Cenozoic vertical motions of the Catalan Coastal Ranges (NE Spain): The role of tectonics, isostasy, and surface transport, *Tectonics*, *23*, TC1004, doi:10.1029/2003TC001511.

[1]Now at Escuela Universitaria de Ingeniería Técnica Topográfica, Universidad Politécnica de Madrid, Madrid, Spain.

0278-7407/04/2003TC001511$12.00

1. Introduction

[2] The Catalan Coastal Ranges (CCR) constitute an excellent geological setting to study the tectonic inversion from compression to extensional tectonics and the interplay between processes operating at different scales, such as lithospheric flexure, fault tectonics and surface processes of erosion and sedimentation. The region located in the present position of the CCR and part of the Valencia Trough (Figure 1) was uplifted during the Paleogene in the context of intraplate compressional tectonics related to the Pyrenean orogeny. This uplifted region is called Catalan Intraplate Chain (CIC) in this paper. Coevally, the Ebro Basin, foreland basin of the Pyrenees, subsided. During the Neogene, the compressional structures of the CIC and the Valencia Trough were overprinted by shorter wavelength, extensional faulting controlling the subsidence of half-grabens and the uplift of the CCR related to the development of the Valencia Trough rift [*Roca et al.*, 1999].

[3] Syntectonic erosion of the Paleogene compressional CIC and its subsequent Neogene extensional exhumation changed the amplitudes and rates of vertical motions [e.g., *Lewis et al.*, 2000]. However, the absence of a complete sedimentary record in some parts of the basins and the lack of precise quantification of amount of rocks eroded during the Cenozoic renders it difficult to asses the size of the CIC and of the Neogene uplifted areas (horsts and rift shoulders) as well as the magnitude of Cenozoic vertical motions.

[4] In combination with surface processes, lithospheric processes such as flexure play an important role in distributing vertical isostatic movements associated with tectonic deformation [e.g., *Small and Anderson*, 1995; *Watts et al.*, 2000], thus affecting the surface mass redistribution by erosion and sedimentation [e.g., *Tucker and Slingerland*, 1994; *Garcia-Castellanos*, 2002]. This isostatic contribution to vertical motions cannot be directly measured and hence it is assessed by numerical methods using a well-constrained data set.

[5] Previous studies constraining the vertical motion history are restricted to periods for which sediments are still preserved [*Bartrina et al.*, 1992; *Vergés et al.*, 1998; *Taberner et al.*, 1999; *López-Blanco et al.*, 2000]. Analyses of the Paleogene sedimentary record interpreted in connec-

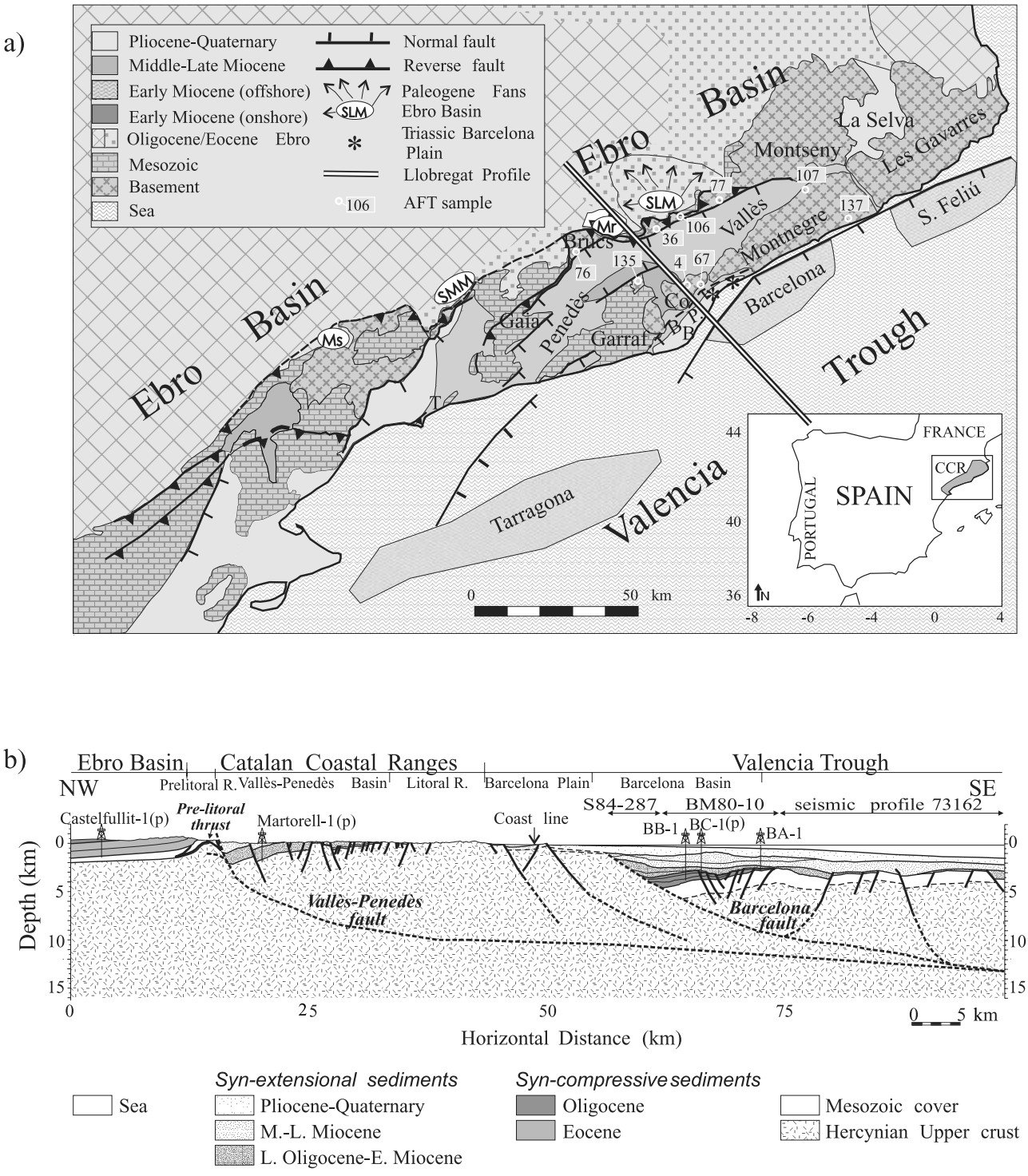

Figure 1. Geological map and study section. (a) Simplified geological map of the Catalan Coastal Ranges and adjacent areas showing main structural units and faults (adapted from *Losantos et al.* [1989]). Bottom right panel shows location within the Iberian Peninsula. Apatite Fission Track sampling locations are shown in the map with the same labels as in Figure 2. Note that the system of thrusts emerging along the Ebro Basin boundary has been plotted as one line. Co., Collserola; B.P., Barcelona Plain; SLM, Sant Llorenç de Munt; Mr, Montserrat; B, Barcelona city; T, Tarragona city. (b) Studied profile: interpreted structural cross section across the central Catalan Coastal Ranges (modified from *Roca et al.* [1999]; see location in Figure 1a). No vertical exaggeration.

tion to tectonic pulses in the CIC [*Jones*, 1997; *López-Blanco et al.*, 2000; *López-Blanco*, 2002] permitted to quantify tectonic subsidence and uplift rates. Constraints on catchment mean elevation and extent [*Jones*, 1997; *López-Blanco et al.*, 2000] as well as flexural effects on vertical motions linked to the Pyrenean growth [*Vergés et al.*, 1998] were also established. However, these quantifications are Paleogene averaged estimates restricted to those periods in which syncompressional sediments are still preserved.

[6] Since no Neogene sediments are found in the Ebro Basin adjacent to the CCR [*Losantos et al.*, 1989; *Barberá et al.*, 2001], studies addressing the Neogene evolution of the vertical motions in the CCR are mainly constrained by data coming from the sedimentary infill of the Neogene grabens. In this way it is possible to quantify basin subsidence and its relation to tectonic activity [e.g., *Bartrina et al.*, 1992] but not mountain uplift. Moreover, sediment budget calculations between volumes of sediment accumulated in these basins and volumes of rock eroded from the bounding ranges, which can potentially constrain surface mass transport, have very limited applicability in the CCR. This is so because these basins were open systems that received material from undetermined sources and transported it toward unconstrained locations [*Gaspar-Escribano*, 2003].

[7] Analyses of lithospheric controls on sedimentary patterns in the CCR area recognize uplift of the Catalan flank due to its erosional unloading and facilitated by extensional faulting and rifting in the Valencia Trough [*Lewis et al.*, 2000; *Gaspar-Escribano et al.*, 2001]. Finally, *Morgan and Fernàndez* [1992] provided different scenarios for the Neogene vertical motions in the CCR compatible with elevation and other geophysical data under the assumption of local isostasy, concluding that the evolution of elevation on the CCR may be explained in terms of extension of a laterally heterogeneous lithosphere. This issue is further explored in this paper with a more refined approach.

[8] The objective of this work is to better understand the Cenozoic interaction between processes involved in vertical motions of the central CCR (Figure 1), and to provide temporal and spatial continuity to periods unconstrained by the available data. For this purpose, we use a numerical model integrating quantitative approaches to fault tectonics, surface transport and flexural isostasy [*Garcia-Castellanos et al.*, 1997, 2002].

2. Geological Evolution of the CCR and Quantitative Constraints

[9] The Catalan Coastal Ranges (CCR) extend over ~250 km along the northeastern coast of Spain and are located between the Ebro Basin and the Valencia Trough (Figure 1a). They present a complex horst and graben configuration, composed by several ENE-WSW to NE-SW-striking blocks generally tilted to the NW. In this work, we study a section that crosses perpendicularly the CCR over Barcelona City (Figure 1b).

[10] The offshore part of the section is derived from basin-scale seismic reflection profiles well constrained by borehole data [*Roca et al.*, 1999]. The onshore part of the section belonging to the CCR is mostly based on field studies [*Bartrina et al.*, 1992; *Cabrera and Calvet*, 1996; *Roca et al.*, 1999; *Lopez-Blanco et al.*, 2000]. Additionally, borehole data as well as a seismic reflection line crossing the Vallès-Penedès half-graben striking parallel to our section and located around 15 km away [*Bartrina et al.*, 1992], further constrain the internal geometry of this basin. Unfortunately, there is no seismic line showing the geometry of the Prelitoral Range (northwestern limit of the CCR). Nevertheless, studies on compressive structures affecting not only the CCR but also the adjoining Ebro Basin, integrated with exhaustive analyses of the Ebro sedimentary fill, help reconstructing the geometry of this part of the section. A number of wells [*Lanaja*, 1987] and structural sections constructed by the combination of reflection seismic lines with field studies [*Vergés et al.*, 1998] were used to compose the northwestern part of the section (Ebro Basin).

[11] There are no deep seismic lines crossing this sector of the CCR that could be used to outline the deep geometry of the faults. However, a crustal-scale reflection line crossing the southwestern CCR shows listric geometry for master normal faults equivalent to the Barcelona and Vallès-Penedès faults of our section [*Sàbat et al.*, 1997]. This observation is consistent with a number of restoration studies proposing such a fault configuration for other sectors of the CCR [*Roca and Guimerà*, 1992; *Gómez and Guimerà*, 1999]. This issue is further discussed below.

[12] The main structures observed in this section from northwest to southeast are:

[13] The Ebro Basin (EB), southern foreland of the Pyrenees, which is filled in this area by Paleogene sediments overlaying a thin Mesozoic cover and locally Hercynian basement. In this work, the Ebro Basin is considered as the foreland basin of the CCR as well, and the terms "distal" and "proximal" are used in relation to the CCR and not to the Pyrenees.

[14] The Prelitoral Range (PR), a narrow strip of Paleogene, NW verging contractional structures that is composed by a Hercynian basement, a thin Mesozoic cover and locally Ebro basin-fill sediments.

[15] The Vallès-Penedès Basin (VPB), an onshore half-graben, limited to the northwest by a major normal fault (Vallès-Penedès fault) that is filled in with Miocene deposits that come from the erosion of the bounding ranges.

[16] The Litoral Range (LR), which in the study section is constituted by the Montnegre-Garraf horst, formed by Paleozoic basement that is covered by Mesozoic sediments toward the southwest. These Mesozoic sediments denote that it is an area slightly deformed during the Cenozoic and that it belongs to the same northwest tilted block covered by the Neogene sediments of the Vallès-Penedès half-graben.

[17] The Barcelona Plain (BP), a set of basement blocks bounded by SE-dipping normal faults (e.g., SE Collserola fault) unconformably covered by Serravallian to Quaternary deposits (except in the vicinity of the Litoral Range [*Fontboté*, 1954]).

Table 1. Fault Configuration Model 5F[a]

Stage	Fault	Location	Start, Ma	End, Ma	Velocity, km/Myr	Displacement, km
Compressional	Th1	Prelitoral Range	54	49	−0.40	−2.0
Compressional	Th2	Prelitoral Range	41	29	−0.40	−4.8
Compressional	Th3	SE Collserola	41	29	−0.45	−0.6
Extensional	BCNf	Barcelona Offshore	28	16	+0.60	+7.2
			15	6	+0.40	+3.6
Extensional	VPf	Vallès-Penedès	25	6	+0.25	+4.7

[a]Start and end refer to fault activity periods. Note velocity change in fault BCNf. Velocities and displacements are measured in the horizontal direction and perpendicular to strike. Minus and plus signs refer to shortening and extension, respectively.

[18] The Barcelona Basin (BB), an offshore half-graben bounded to the northwest by a master normal fault (the Barcelona fault). It is constituted by a roughly continuous sequence of Lower Oligocene to Present sediments that overlay Mesozoic sediments.

[19] The Cenozoic evolution of the Catalan Coastal Ranges and surroundings can be subdivided into two stages [e.g., *Roca*, 1996]: (1) Paleogene compressional stage (Late Paleocene-Early Oligocene) and (2) Neogene extensional stage (Late Oligocene-Present).

2.1. Paleogene Compressional Stage (Late Paleocene-Early Oligocene)

[20] The CCR developed during the Paleogene in the context of the Pyrenean orogeny, after tectonic inversion of former Mesozoic basins [*Roca*, 1996]. A ~100 km-long and 50–60 km-wide area occupied in the present by the CCR and the NW margin of the Valencia Trough underwent uplift and erosion [*Roca et al.*, 1999; *López-Blanco et al.*, 2000], forming the so-called Catalan Intraplate Chain (CIC).

[21] The Paleogene evolution of the CIC is extensively analyzed by *López-Blanco et al.* [2000] by combining multiple data sources (sedimentologic, structural, stratigraphic, palynologic and paleomagnetic data) based on surface studies of Ebro Basin fill deposits. According to these authors, deformation of the CIC was characterized by the growth of a system of NW directed thrusts and folds, which relicts crop out close to the eastern Ebro Basin margin (Figure 1). In the studied transect, the first contraction pulses occurred during the Paleocene-Eocene boundary [*López-Blanco*, 2002], reactivating (with reverse motion and a sinistral strike-slip component [*Guimerà*, 1984]) a long-lived weakness zone that controlled the opening of the Mesozoic basin and subsequently of the Miocene Vallès-Penedès Basin. The shortening along the frontal part of the CIC generated by this first thrust system (Th1 in Table 1) is estimated in ~2 km and lasted until the end of Ypresian (~49 Ma [*López-Blanco et al.*, 2000]). The next deformational phase (Lutetian-Bartonian) was characterized by the development of a syncline-anticline pair that folded older structures located in the frontal CIC and implied moderate shortening [*López-Blanco*, 2002]. As no outcropping thrusts constrain this stage, it is not included in our model. When the accumulated strain overcame a certain threshold, thrusting restarted with the development of a low-dip, out-of-sequence thrust that was active from Bartonian to Early Oligocene (Th2 in Table 1 [*López-Blanco et al.*, 2000]). This thrust implied a shortening of ~4 km and uplifted a broader region than the first one, between 0.7 and 1.2 km above the Ebro Basin [*López-Blanco et al.*, 2000]. Southeast of this area, only minor faulting occurred, except in the vicinity of the present coastline, where strong compression took place at least during the early Late Oligocene [*Parcerisa*, 2002]. In our study we propose a configuration for this stage comprising the activity of a third thrust (Th3 in Table 1) located in the hanging wall of thrust Th2 (section 5.2).

[22] Maximum amounts of Paleogene exhumation of the CIC up to 1.3 km (Figure 2) are estimated from apatite fission track (AFT) studies [*Juez-Larré*, 2003] combined with thermokinematical modeling [*Gaspar-Escribano*, 2003]. Independent calculations of Paleogene exhumation based on balancing of Ebro deposits volume reduce this amount to ~0.8–1 km [*López-Blanco et al.*, 2000].

[23] Coeval to this deformation history in the CIC, the Ebro foreland and Barcelona basins developed. The first one was filled with significant amounts of synorogenic terrigenous deposits (partly marine until the Bartonian; [*Vergés et al.*, 1995]) that generated significant topography within the basin during the Paleogene [*Coney et al.*, 1996]. Nowadays the age of the outcropping Ebro Basin deposits increases from the Catalan margin (Eocene) to the center of the basin (Oligocene-Miocene). Their distribution and NW-tilted bedding (Figure 1b), suggest that deposition actually took place in the easternmost Ebro Basin during Oligocene, but the missing (Oligocene-Miocene) sediments were eroded away in a later stage [e.g., *Anadón et al.*, 1989].

[24] The Barcelona Basin developed in the hinterland of the CIC. Tectonosedimentary analyses of the Barcelona Basin infill [*Roca et al.*, 1999] show that its lower sequence (Upper Eocene-Oligocene) was deposited prior to the Neogene rifting phase and it is coeval with compressional deformation in the CIC. The evolution of this basin is poorly constrained. Its geometry (see Figures 1b and 3) could be associated to the extensional development of a half-graben resulting from the transcurrent motion between the Ebro Basin block and the CIC. Alternatively, it can be considered as a piggyback basin developing under the compressional tectonic regime that also affects the Ebro margin. In this paper we followed the second option, which is supported by two points: (1) The constant thickness of the sedimentary packages, not showing the thickening toward the active fault

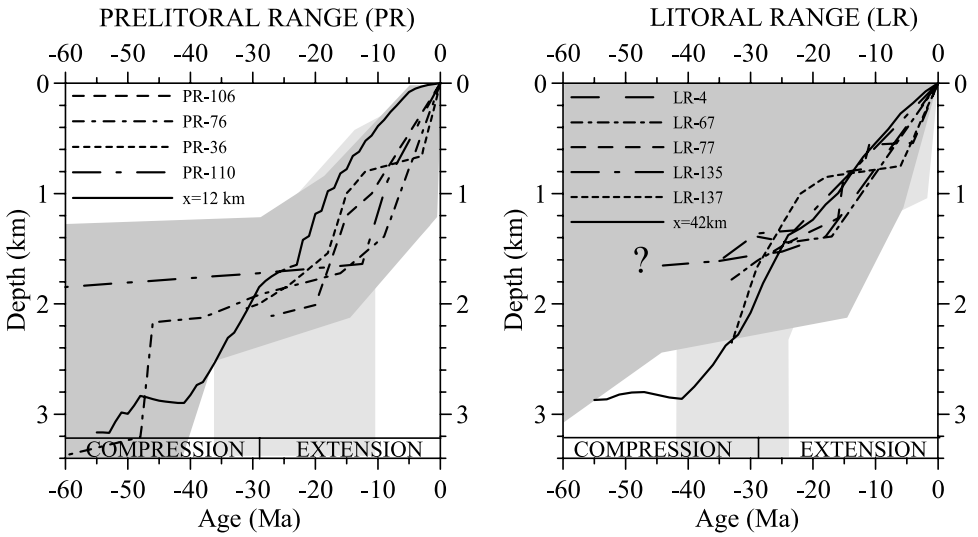

Figure 2. Interpreted apatite fission track thermal history for different locations in the Prelitoral and Litoral (Garraf-Montnegre horst) ranges (modified from *Juez-Larré* [2003]). A geothermal gradient of 25°C/km and 37°C/km for the compressional and extensional stages respectively were used to convert temperature into depth (respect to the local surface in each moment [*Gaspar-Escribano*, 2003]. Sampling locations in Figure 1 (same numbering). Thick lines represent results from Model 5F (section 4.3). Shaded areas give the error margin of the AFT method.

characteristic of the half-grabens [*Roca et al.*, 1999]; and (2) Occurrences of Oligocene sediments in the footwall block of the Barcelona Basin affected by compressive (and not extensive) features (Turó de Mongat-Barcelona Plain [*Parcerisa*, 2002]). In any case, further research should be carried out to discern which alternative is the most plausible.

2.2. Neogene Extensional Stage (Late Oligocene-Present)

[25] From Late Oligocene onward, extensional tectonics mainly driven by the Vallès-Penedès and Barcelona master faults led to the dismantling of the CIC and rearrangement of the area into horsts and grabens (Figure 1b). Main activity of these faults took place during latest Oligocene-Langhian and was accompanied by strong tectonic subsidence, which initially lowered topography and later created accommodation space that was gradually infilled by detritic deposits (mainly in the vicinity of the fault planes). Secondary faults bounding the grabens (e.g., SE Collserola fault) involved lesser displacement and therefore were not included in our model. The main marine transgression started during late Aquitanian (~22 Ma) in the Barcelona Basin [*Roca et al.*, 1999] and gradually progressed from SE to NW reaching the Vallès-Penedès Basin during Late Burdigalian [*Cabrera and Calvet*, 1996]. These ages of the continental-marine transitions provide paleoelevation constraints to the model. Fault activity decreased during Middle-Late Miocene and concentrated in the master faults. Only continental sedimentation continued in the Vallès-Penedès Basin, gradually consuming the accommodation space. In turn, large accommodation space was still available in the Barcelona Basin, where marine deposition with significant lateral supply dominated [*Cabrera and Calvet*, 1996]. By Latest Miocene (Messinian), compressive inversion of previous normal faults (B. Gelabert et al., Neogene evolution of the Valencia Trough and Algerian Basin: From extension to inversion, manuscript in preparation, 2003) together with the Mediterranean sea level low-stand [*Clauzon et al.*, 1996] resulted in an uplift of the CCR, which were submitted to large, nonquantified erosive processes. From Pliocene to Present, the Vallès-Penedès fault was inactive [*Masana*, 1994] and only the Barcelona and SE Collserola faults show moderate tectonic activity in our transect [*Olivera et al.*, 1992]. Consequently, the already uplifted CCR did not subside again. While little amounts of Pliocene-Quaternary sediments were deposited in the Vallès-Penedès basin [*Martinell*, 1988], significant amounts of sediments covered both the Barcelona Basin and Plain (Figure 1a).

[26] In the Ebro Basin deposition continued until its opening to the Mediterranean Sea in Middle-Late Miocene times, when widespread erosion took place [*Riba et al.*, 1983]. Consequently Neogene sediments are lacking in the easternmost Ebro Basin or present in insignificant amounts (Figure 1) [*Anadón et al.*, 1989; *Barberá et al.*, 2001].

[27] Constraints on amounts of Neogene exhumation of the CCR can be derived from studies integrating AFT data and tectonothermal modeling [*Gaspar-Escribano*, 2003; *Juez-Larré*, 2003]. AFT thermal histories show a marked cooling event during Neogene [*Juez-Larré*, 2003], which reveals important exhumation (up to 2 km) of pre-Cenozoic rocks in the Prelitoral and Litoral ranges [*Gaspar-Escribano*, 2003].

2.3. Preliminary Partial Restoration

[28] The evolutionary scenario described above was derived from a number of studies using different techniques

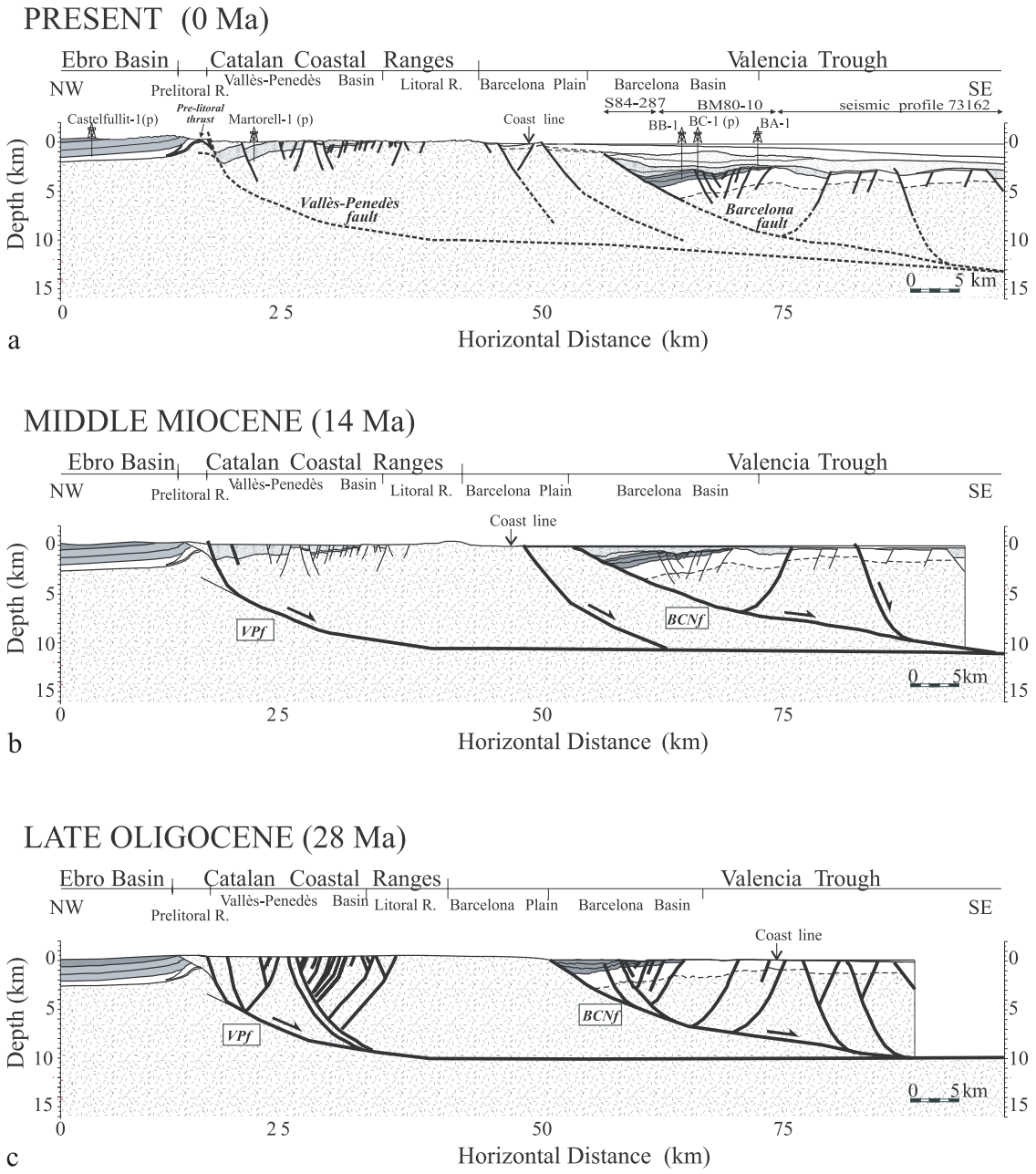

Figure 3. (a) Partial restorations of the transverse Catalan Coastal Ranges cross section (see Figure 1) at five times: (b) beginning end of the postrift stage (Middle Miocene), (c) beginning of the synrift phase (Late Oligocene), (d) end of the compressional stage (Early Oligocene), (e) n intermediate stage during the development of the CIC (Middle Eocene), and (f) the beginning of the Paleogene compressional stage (Early Eocene). The right limit of the section is fixed as reference point. Thick and thin, solid lines stand for active and inactive faults, respectively. Same fault labeling as in Table 1.

and addressing different segments of the study section and/or different time-spans of its evolution. In order to provide a first-order picture of the tectonic evolution of the central CCR, integrating the data described above altogether and in an internally consistent manner, and eventually to gain new insights on the evolution of the area, we carried out a partial restoration exercise of the section constrained by all that geological and geophysical information.

[29] Figure 3 gives, apart from the present-day section (as in Figure 2), five partially restored sections across the CCR for Middle Miocene, Late Oligocene, Early Oligocene, Middle Eocene and Early Eocene. Deep geometry of normal faults and partial restorations of these faults (Middle Miocene and Late Oligocene) were performed assuming an inclined shear algorithm with shear angle of 65° [e.g., *Gibbs*, 1983]. Note that whereas during the synrift

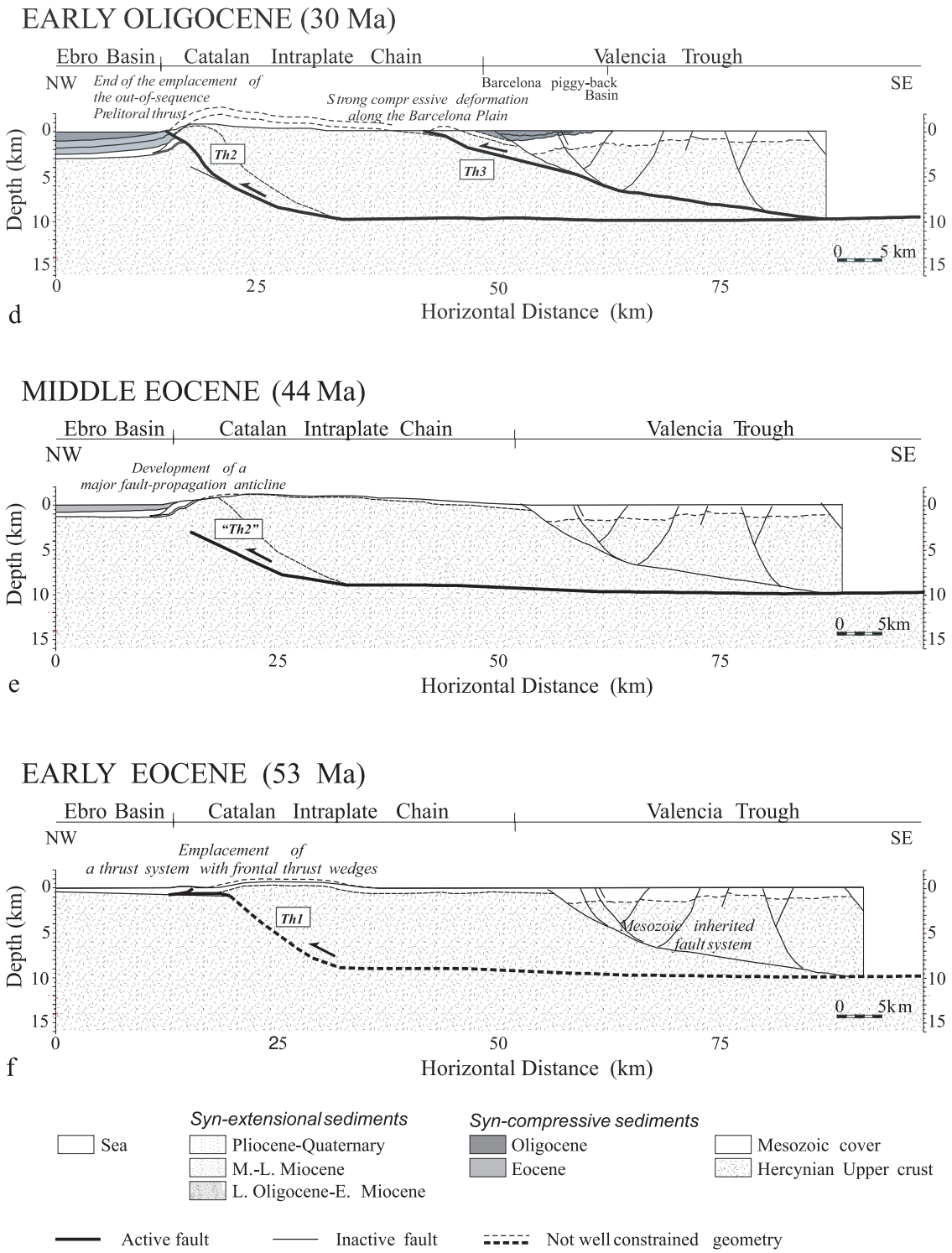

Figure 3. (continued)

phase all normal faults were active (Late Oligocene section), during the postrift phase only the faults involving largest displacement were active (Middle Miocene section). It is also clearly shown that deposition started earlier in the Barcelona Basin than in the Vallès-Penedès Basin. According to this restoration model, total extension amounted 11.3 km (7.1 and 4.2 km during the synrift and postrift phases, respectively). Reverse faults, active during the compressional phase, were restored assuming a flexural slip unfolding mechanism [e.g., *Hossack*, 1979]. In this case, a third thrust (Th3) with respect to the evolutionary scenario proposed by *López-Blanco et al.*

[2000] was introduced in the hinterland of the CIC (see justification in section 4.1). Total shortening amounted 7.2 km. During the Early Oligocene, deposition took place in the piggyback Barcelona Basin. At the same time, an out-of-sequence thrust (Th2) was emplaced over Ebro Basin sediments. In the early stages of the model, deposition occurred in the Ebro Basin only. During Middle Eocene, a blind thrust system "Th2" developed, folding Ebro Basin deposits (fault-propagation fold). At the beginning of the evolutionary model (Early Eocene), compressive deformation involved the activation of a frontal thrust (Th1). Mesozoic sequences that were gradually eroded during the compressional phase were also included in the restoration according to quantitative constraints (see section 2.2 and the work of *López-Blanco et al.* [2000]). The sharp variation on thickness of Mesozoic (Upper Jurassic and Lower Cretaceous) sequences, most evident between the areas corresponding to the offshore and onshore at present (Figure 3, 53 Ma), suggests that the Barcelona fault system played an active role in the evolution of the area prior to the Cenozoic [*Roca and Guimerà*, 1992], controlling the development of extensional basins during Late Jurassic- Early Cretaceous [e.g., *Salas and Casas*, 1993]. Accordingly, the Barcelona fault would be a feature inherited from the Mesozoic. An older activation of this fault system cannot be surely established.

[30] This restoration exercise provides a reference evolutionary model consistent with both depositional and fault activity patterns inferred from a variety of geological and geophysical data obtained by different techniques. However, it contains a number of deficiencies, such as (1) it cannot provide quantitative constraints on amounts of erosion for the entire geological evolution, (2) it cannot account for vertical motions related to isostasic compensation to mass redistribution (3) it lacks a process-based explanation for the evolution of topography and particularly for the role of fault tectonics, isostasy and surface transport. Below, we use of a numerical model to address these issues. For the sake of simplicity and to save computation time, we will reduce the number of faults included in the model by considering the ones that involve larger displacements only. For the sake of the clarity required for the interpretation of the vertical motion evolution, we will adopt a vertical shear approach. Nevertheless, we will discuss the implications that these assumptions have on our results.

3. Numerical Model and Parameterization

3.1. Model Description

[31] In order to quantitatively link processes active during Cenozoic vertical motions in the study area, we use a numerical model integrating fault tectonics, isostasy and surface transport [*Garcia-Castellanos et al.*, 1997, 2002]. The model allows for the coexistence of multiple active fault-blocks, finite fault activity periods, and both normal and reverse motions on faults. Tectonic transport in the upper crust was simulated by a number of fault blocks that deform following a vertical shear approach: The vertical thickness of the hanging wall block is preserved during fault movement. Flexural isostasy is implemented adopting a thin-elastic plate [*Turcotte and Schubert*, 2001] compensating for the load contrasts generated by mass redistribution (caused by tectonic or surface mass transport). Lateral rigidity variations of the lithosphere were taken into account via changes in effective elastic thickness (T_e), which is assumed to be constant through time. Hidden loads related to deeper processes in the upper mantle, as well as vertical forces or moments in the limits of the model [e.g., *Sheffels and McNutt*, 1986] can be incorporated to refine the distribution of loads flexing the plate.

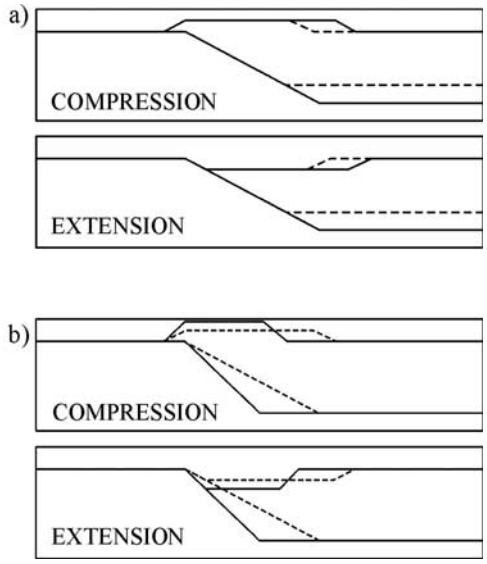

Figure 4. (a) Cross-section cartoon showing the effect on basin and mountain geometries of fault detachment depth. Dashed and solid lines are for shallow and deep detachment levels, respectively. (b) Fault dip angle. Dashed and solid lines are for small and large dip angles, respectively.

[32] Surface erosion and sedimentation are carried out in two different ways: (1) at linear rate, erosion rate is proportional to elevation in continental areas and sedimentation rate is constant below sea level, and (2) diffusive transport, sediment flow is proportional to the slope along the profile, and erosion and sedimentation rates are proportional to the curvature of elevation [e.g., *Flemings and Jordan*, 1989]. In both cases, the respective transport parameters are taken constant through time.

[33] The model provides predictions on the evolution of topography, plate deflection, geometry of fault blocks and amounts of material deposited or eroded. Sea level changes are taken into consideration as well (adopting the curve of *Haq et al.* [1987], modified for the Messinian Mediterranean sea level low stand).

3.2. Effect of Fault Geometry on Basin and Mountain Configuration

[34] The shape of a basin or mountain resulting from tectonic transport along a fault plane, depends on the geometry of the fault. Figure 4 schematically shows the effect of the depth of detachment and dip angle of the fault

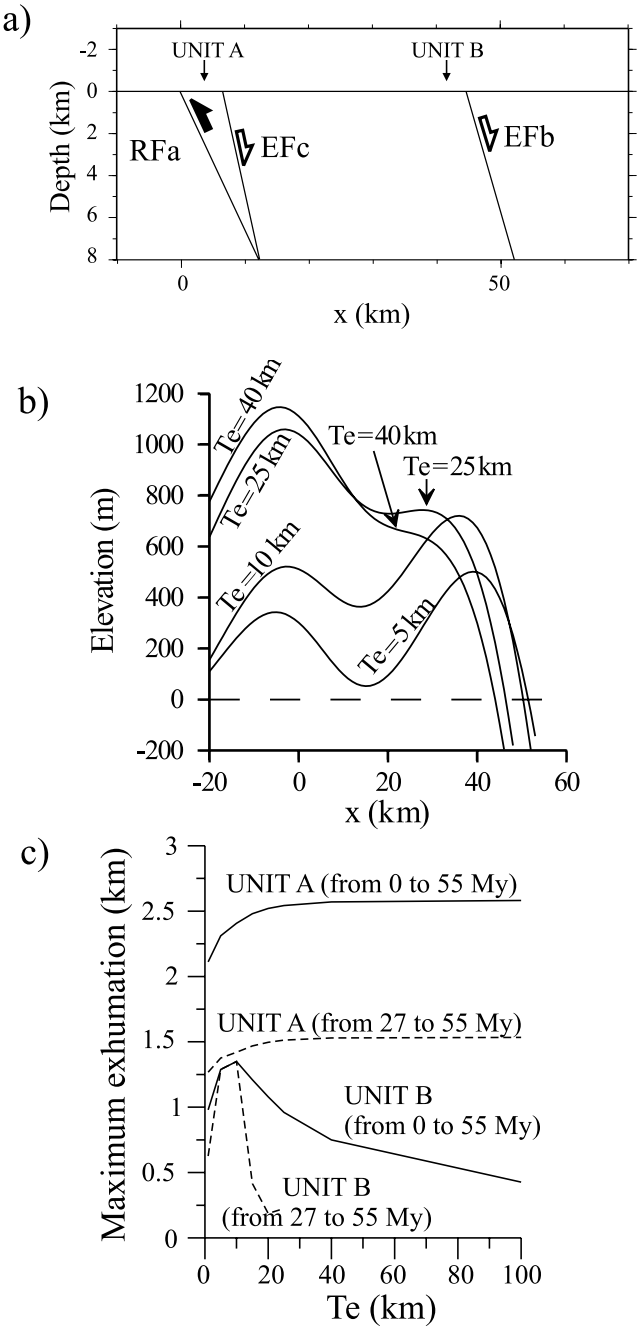

Figure 5. Results of the synthetic Model 3F illustrating the relation between rigidity (via T_e) and measurable magnitudes. (a) Model 3F setup. Units A and B refer to locations in which basement crops out and exhumation can be measured. Unit A is equivalent to Prelitoral Range, and Unit B is equivalent to Litoral Range (Garraf-Montnegre horst). (b) Elevation profile across the Litoral Range for different T_e values. Horizontal line indicates sea level. High Te values lead to water divide vanishing and exaggerated scarp retreat. (c) Maximum cumulative exhumation onshore versus T_e for units A and B. Thick lines represent total exhumation after 55 Myr of model evolution and dashed lines represent exhumation only during extensional phase (i.e., from 27 to 55 Myr after the beginning of the model).

Table 2. Fault Configuration Model 3F

Stage	Fault	Start, Myr	End, Myr	Velocity, km/Myr
Compressional	RFa	0	25	−0.32
Extensional	EFb	27	47	+ 1
Extensional	EFc	28	47	+0.25

on the topography resulting after extension or shortening. For the same amount of extension and dip angle, the deeper the detachment level, the wider the basin. Similarly, the topography created by thrusting will be narrower for shallower detachment levels (Figure 4a). As for extension, the higher the dip, the deeper and narrower the basin (normal motion), and conversely for compression, the higher and narrower the topography created (reverse motion) (Figure 4b).

[35] During the modeling process, fault parameters unconstrained by seismics or field studies (i.e., fault deep geometry) were adjusted to take into account the above criteria in order to fit hanging wall blocks (basin and mountains) and fault geometries.

3.3. Model Parameterization

[36] In order to estimate the sensitivity of modeling predictions (e.g., amounts of exhumation, present-day geometries) to different parameters, a number of tests were carried out using a simple model configuration consisting of three faults, diffusive surface transport, and flexural isostasy (Model 3F; Figure 5a and Tables 2 and 3). Topographic profiles after 55 Myr are shown in Figure 5b for different T_e values. As T_e values increase, topography smoothens and the coastline migrates landward. Thus low T_e values (T_e < 15 km) are necessary to predict a clear topographic maximum near the coastline.

[37] Model 3F was also used to test the relationship between T_e and onshore basement exhumation. Figure 5c displays variations of cumulative exhumation (from the beginning of the model until the time considered) with T_e for the two tectonic blocks (Unit A and Unit B in Figure 5a). The values displayed correspond to the maximum exhumation accumulated after 55 Myr in the onshore basement outcrops. Exhumation values found in presently submerged domains are not included in the Figure 5 because of the lack of thermochronological measurements

Table 3. Model 3F Parameters

Parameter	Value
Modeled time span	55 Ma-Present
Length of the model	300 km
Depth of detachment	16 km
Mantle density	3250 kg m^{-3}
Basement density	2850 kg m^{-3}
Sediment density	2200 kg m^{-3}
Diffusive erosion constant	5×10^6 m^2 Myr^{-1}
Continental background constant erosion rate	0 m (m $Myr)^{-1}$
Marine sedimentation rate	0 m Myr^{-1}

in these regions. Cumulative exhumation of Units A and B are similar for low T_e values only ($5 < T_e < 15$ km in Figure 5c), and during the extensional phase. These qualitative relations between T_e and topography and between T_e and total cumulative exhumations have been found also valid for other combinations of surface transport parameters.

[38] In conclusion, these tests show that, regardless the choice of transport parameters, setting low T_e values around the shoreline correctly predicts a topographic maximum separating two basins and similar exhumation values in Units A and B during the extensional phase. These results are applicable to our study area taking as analogue to Units A and B the Prelitoral Range and the Litoral Range, respectively.

4. Evolutionary Model

4.1. Modeling Setup

[39] In a more detailed model for the evolution of the CCR (Model 5F), we incorporate five faults (Table 1). A 300-km-long elastic plate with 0.5 km node spacing was used to carry out flexural calculations. Whereas the length of the model is adequate for computing regional compensation (according to the T_e distribution presented below [see also *Gaspar-Escribano et al.*, 2001]), the node spacing provides sufficient spatial resolution for identifying (flexural) effects related to fault-block motions.

[40] A lateral T_e variation was imposed on Model 5F (Figure 6). A low T_e value (5 km) was defined near the shoreline (as inferred from the parameterization, see section 3.3), and extended seaward [*Watts and Torné*, 1992]. T_e values gradually increase beneath the CCR toward the Ebro Basin, where a value of 25 km [e.g., *Millán et al.*, 1995] was used. The load imposed by the Pyrenees over the Iberian micro-plate was incorporated in the model via a vertical force located in the left (northwestern) free boundary of the model. The value of this force (Table 4) was taken from *Gaspar-Escribano et al.* [2001].

[41] The model ran from 55 Ma (Paleocene-Eocene boundary) to 0 Myr (Present-day) in time intervals of 1 Myr. The initial topography was defined at sea level in the Ebro Basin, increasing gradually to 0.2 km in the present-day offshore areas [*Puigdefábregas et al.*, 1986].

[42] Only major faults were included in the model, thus ignoring faults involving small displacements. Fault parameters, constrained by geological and geophysical data, are listed in Table 1. For the case of the reverse faults, these parameters are derived by extrapolation of surface data, as it is explained in the following: As thrust Th1 is related to a Mesozoic extensional fault linked to the Vallès-Penedès weakness zone (see section 2.1), it has a steep near-surface

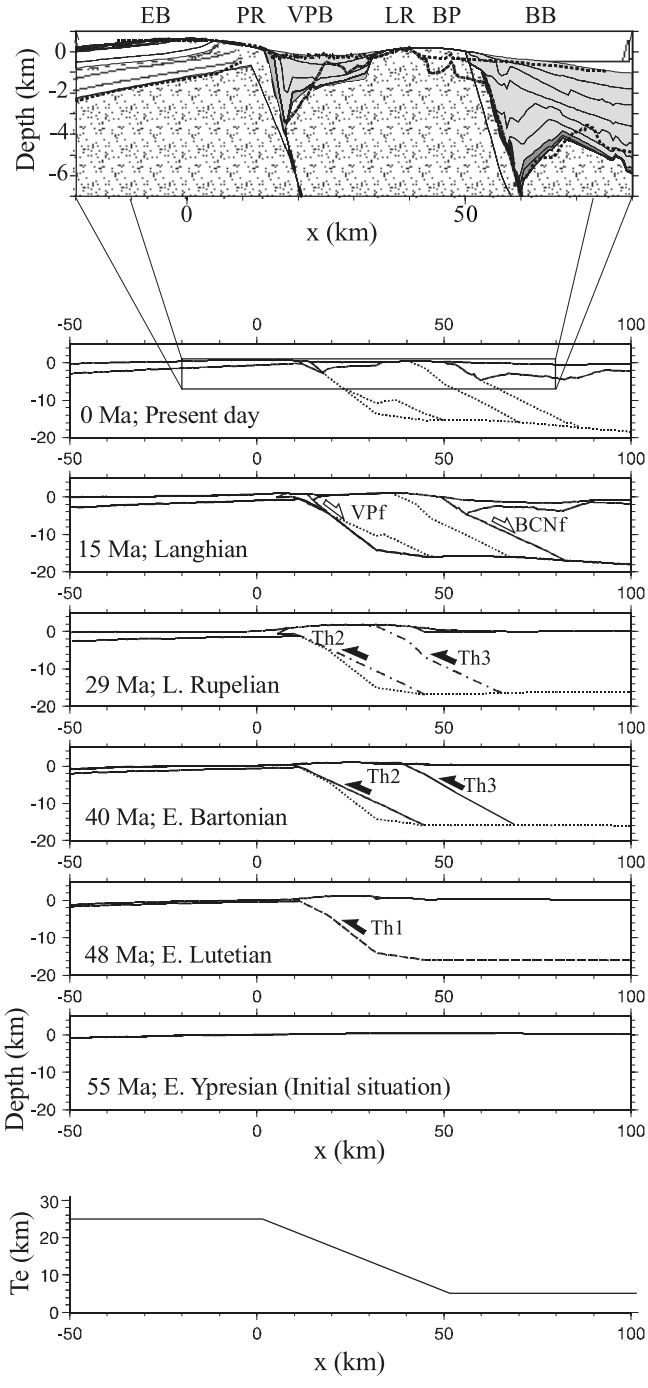

Figure 6. Upper crustal geometries showing fault blocks and sediment packages in six different representative moments derived from Model 5F. Thick lines represent active faults, top of basement, and topography. Dashed lines stand for faults that stopped moving 1 Ma. Dashed-dotted lines refer to faults which will become inactive within 1 Myr. Dotted lines represent inactive faults. Fault nomenclature as in Table 1. Blow up of present-day configuration. Dark and light shading represent syncompressive and synextensional sediments, respectively. Thick dotted lines represent observed topography, bathymetry, and base of Tertiary sediments. Thin black lines are time lines showing sediment bedding. EB, Ebro Basin; PR, Prelitoral Range; VPB, Vallès-Penedès Basin; LR, Litoral Range; BP, Barcelona Plain; BB, Barcelona Basin. The bottom panel shows the T_e configuration used in Model 5F (see section 4.1).

Table 4. Model 5F Parameters

Parameter	Value
Modeled time span	55 Ma-Present
Length of the model	300 km
Depth of detachment	16 km
Mantle density	3250 kg m^{-3}
Basement density	2850 kg m^{-3}
Sediment density	2200 kg m^{-3}
Vertical force (Pyrenean load at x = −100 km)	$-2.5 \times 10-^{12}$ N m^{-1}
Diffusive erosion constant	5 10^6 m^2 Myr^{-1}
Continental background constant erosion rate	0.05 m (m Myr)$^{-1}$
Marine sedimentation rate	90 m Myr^{-1}

dip (∼40°) and connects in depth with the Vallès-Penedès fault [*Roca and Guimerà*, 1992; *Roca et al.*, 1999]. Alternatively, we confer a flatter geometry in depth to thrust Th2, according to the prolongation of its near-surface dip (∼20° [*López-Blanco et al.*, 2000]). In addition to the documented thrusts [*López-Blanco et al.*, 2000], we incorporate a third thrust in the back limb of the CIC (Th3 in Table 1), which is not directly captured by seismic lines. This allows reducing topographic gradients and accommodation space in the hinterland, and minimizes the amounts of erosion and sedimentation. Consequently, a limited amount of sedimentation (as revealed by AFT data) and restricted only to the present onshore areas [*Roca et al.*, 1999] will be predicted by the model (see section 5.2 for further discussion on thrust Th3). Regarding the extensional stage, the geometry of the Barcelona and Vallès-Penedès normal faults and their periods of activity are constrained by seismic profiles crossing the respective half-grabens [*Bartrina et al.*, 1992; *Roca et al.*, 1999]. These data suggest a listric fault geometry that soles out in a detachment level of depths of 12–16 km [*Roca and Guimerà*, 1992; *Roca et al.*, 1999]. The further continuation of this detachment level toward the axial part of the Valencia Trough cannot be certainly established from the data. For the sake of simplicity, in our modeling we assume that all faults connect with one single intracrustal detachment level at 16 km depth, and that no simultaneous compression and extension in the CCR and Valencia Trough occurs. Although further complications of the assumed setting have not been tested, the results show that these approaches are sufficient to explain the evolution of erosion and sediment accumulation in the study area. Other modeling parameters are listed in Table 4.

[43] In order to create accommodation space for marine sedimentation during the extensional phase, an additional load of 1×10^8 N m^{-2} was introduced to the southeast of the Barcelona half-graben (between x = 62 km and x = 100 km), where no evidences of major faulting are found to account for the observed important subsidence. This load was gradually emplaced from 25 to 1 Ma and is probably related to other rift-related processes not explicitly accounted for in this study, such as tectonic subsidence due to mechanical stretching and thermal thinning of the lithosphere and postrift thermal subsidence [*Negredo et al.*, 1999]. This lithospheric configuration is supported by wide-angle reflection and refraction seismics showing crustal thinning underneath the CCR [*Gallart et al.*, 1994] and gravity-geoid anomaly modeling indicating strong lithospheric thinning [*Ayala et al.*, 1996].

4.2. Model Evolution

[44] Figure 6 gives results of Model 5F showing the evolution of the studied section at six different time steps. According to the model, shortening by 2 km along the fault labeled as Th1 uplifts a ∼20 km wide area that supplies sediments to the Ebro Basin (Figure 6, 48 Ma). Subsequently, thrusts Th2 and Th3 broaden the uplifted area toward the southeast, preventing major sedimentation in the hinterland during the Eocene (Figure 6, 40 and 29 Ma).

[45] These faults involve a shortening of 4.8 and 0.6 km, respectively. During the Late Oligocene (Figure 6, 29 Ma), the CIC presents its highest topography. Then the tectonic regime changes to extension (at 28 Ma) and the older reverse fault systems are reactivated as normal faults, reducing the topography created during the compressional phase and controlling the subsidence of the Barcelona and Vallès-Penedès half-grabens. At 22 Ma, the Barcelona Basin records the start of a marine transgression that lasted until the present-day (with the exception of the Messinian). In turn, continental deposition prevails in the Vallès-Penedès Basin, where a short marine episode is predicted between 9 and 5 Ma. During the Miocene, extension progresses (Figure 6, 15 Ma) and the proximal parts of the Ebro Basin and the Prelitoral and Litoral ranges are isostatically uplifted. In the model, fault activity ceases at 6 Ma (Messinian), and total horizontal extension in the CCR amounts to 15.5 km, subdivided in 10.8 km for the Barcelona fault (BCNf) and 4.7 km for the Vallès-Penedès fault (VPf). The modeled present-day situation (Figure 6, 0 Ma and top) shows a well-defined horst and graben structure, close to the geometry inferred from geological and geophysical data (see Figure 1b).

4.3. Evolution of Vertical Motions: Effects of Isostasy, Erosion, and Sedimentation

[46] In the following description of our modeling results, the predicted change in topography at any given location of the model is separated into three components [e.g., *Abbott et al.*, 1997] that verify the following relation:

$$dT = FTU + dS + IU,$$

where dT is the change in elevation relative to the present sea level; FTU is the vertical rock movement induced by fault activity (positive means uplift and negative subsidence); dS is the thickness of eroded (negative) or deposited (positive) material; and IU is the vertical isostatic motion (negative means subsidence).

4.3.1. Compressional Stage

[47] The model evolution is consistent with a phase of thrust-controlled tectonic uplift leading to the development of the CIC between 55 and 29 Ma (Figure 7; x = 12 and 42 km). Paleogene syncompressional topography growth was partially compensated by erosion of the uplifted areas

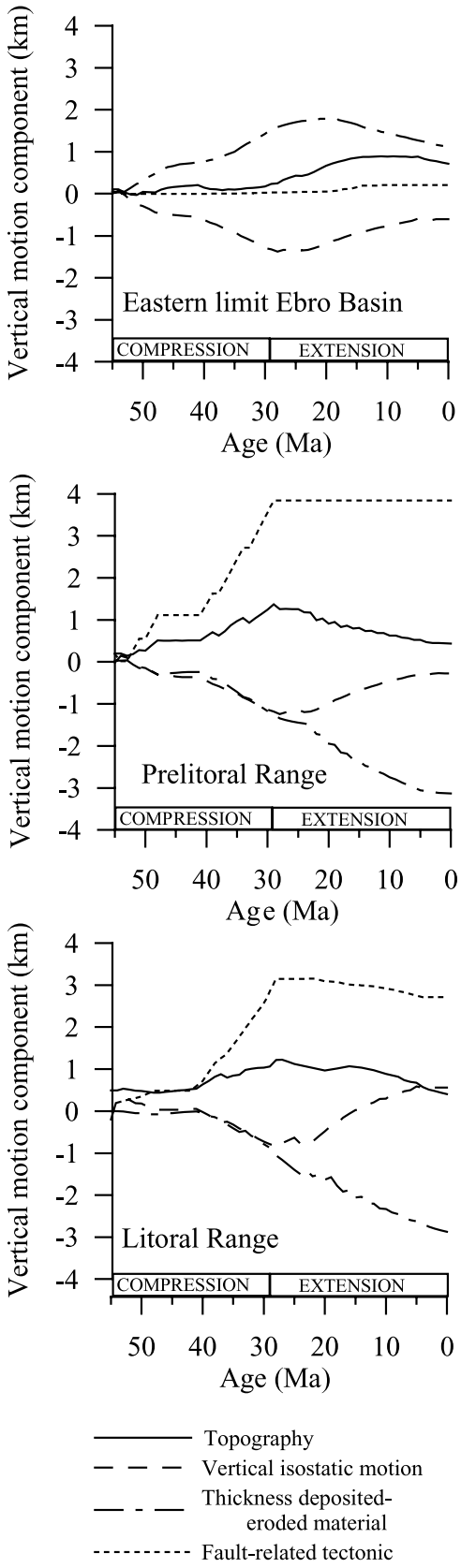

(up to 1.3 km) and their isostatic subsidence (up to 1.2 km), resulting in a 1.2–1.9 km high CIC by the early Oligocene (30 Ma) (initial topography was 100 m). In the back limb of the CIC a relatively thin (0.5 km) sedimentary layer was deposited prior to 41 Ma (Figure 6) which was partially eroded by the end of the compressional stage, after the activation of thrusts Th2 and Th3.

[48] Flexural isostasy controls vertical motions in the Ebro Basin during the compressional phase (Figures 7 and 8). According to our modeling predictions, the basement underlying the Ebro Basin bends toward the NW in response to Pyrenean loading, but not toward the SE underneath the CIC. Thus the topographic loading effect of the CIC is insufficient to generate a significant flexural response in the SE margin of the Ebro Basin.

4.3.2. Extensional Stage

[49] During Late Oligocene-Neogene, a drastic change in vertical motions trends was recorded as a consequence of the extensional tectonics and structural rearrangement of the CIC (Figures 7 and 8). Activity of the Barcelona and Vallès-Penedès master faults lowered the topography inherited from the compressional phase and produced strong tectonic subsidence in the hanging wall domains (up to 5 km; Figure 8). As calculated by the model, flexural uplift by 0.7–1.2 km opposed (but never overcame) this subsidence, and affected the whole area under consideration. According to our predictions, the Barcelona fault controlled flexural uplift patterns not only in the adjacent Barcelona footwall but also in the more distant Vallès-Penedès footwall (Figure 8). This is evidenced by a general diminution in isostatic uplift recorded from the synrift to the postrift stage and related decrease on the rate of extension of the Barcelona fault (Figure 8).

Figure 7. Model 5F results. Temporal evolution of topography corrected for sea level variations (thick line) and the three main parameters that control its evolution: fault tectonics (short-dashed line), flexural isostasy (long-dashed line), and surface transport (thickness of deposited and eroded material; dash-dotted line). Three locations are considered: the easternmost Ebro Basin (x = 2 km), the Prelitoral Range or frontal part of the CIC (x = 12 km), and Litoral Range or hinterland of the CIC (x = 42 km). Topography is always related to present-day zero sea level. Positive and negative values of fault tectonic curve slopes respectively represent uplift and subsidence in the time interval considered. Negative deflection curve slopes denote progressive plate sinking, which implies creation of accommodation space in sedimentary basins and crustal thickening in the orogens. Positive slopes indicate plate uprising, referred to as flexural uplift. Positive and negative values of surface transport curves refer to amounts of deposited and eroded material from the beginning of the model until a given time, respectively. In the case of sedimentary basins, positive slopes (as during Paleogene in x = 2 km) reveal actual deposition, while negative slopes (as during Miocene in x = 2 km) denote erosion of the sedimentary cover (deposited in an earlier stage).

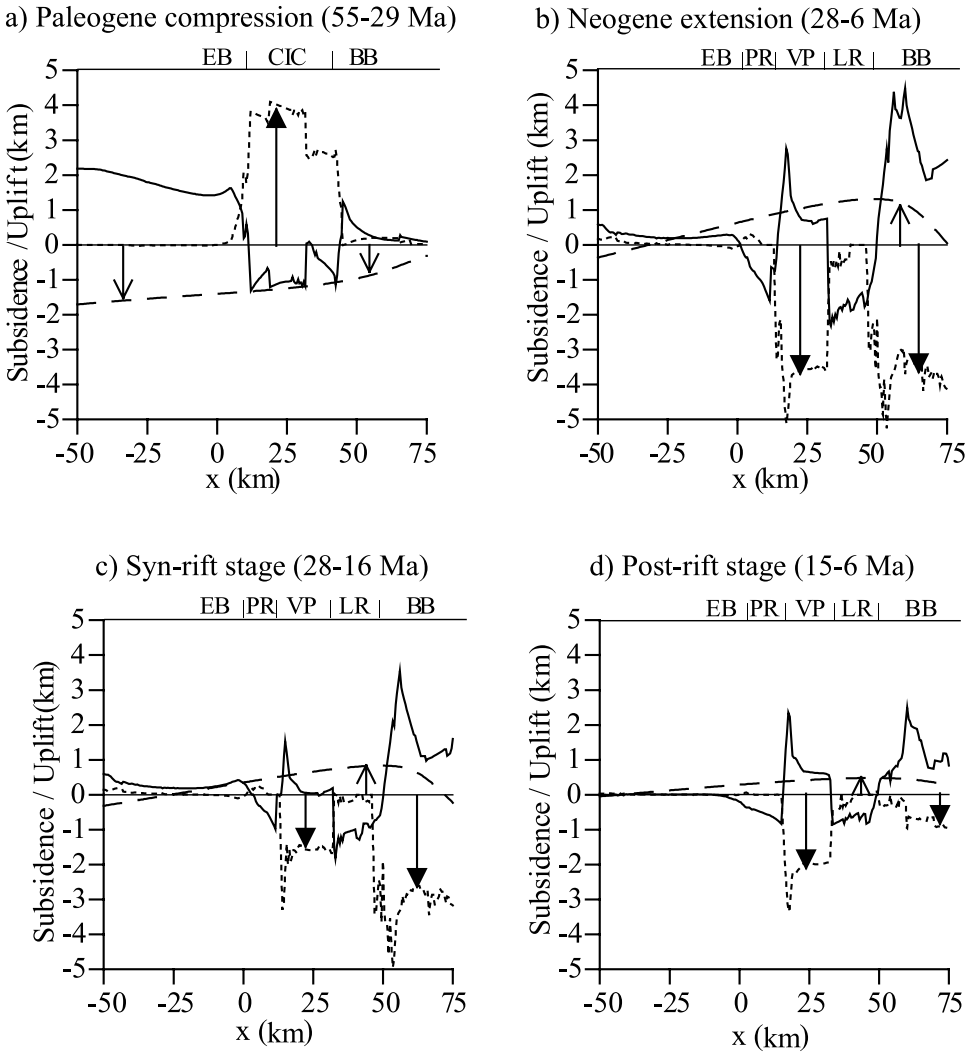

Figure 8. Relative contributions to vertical motions in different time intervals for the study section. Solid line represents thickness of deposited (positive) and eroded (negative) material, long-dashed line represents net flexural isostatic uplift (positive) or subsidence (negative), and short-dashed line represents fault-related tectonic uplift (positive) or subsidence (negative). Solid arrows mark fault-related tectonic uplift and subsidence, and open arrows mark flexural isostatic uplift or subsidence. (a) Compressional phase (55–29 Ma). (b) Extensional phase (28–6 Ma). (c) First part of the extensional phase (28–16 Ma). (d) Second part of the extensional phase (15–6 Ma).

Between 2.6 and 4.6 km of sediments infilled the accommodation space created by fault-related tectonic subsidence in the Vallès-Penedès and Barcelona basins, respectively (Figure 8). These sediments were supplied partly by erosion of the bounding ranges and partly by a marine sediment source (the later mostly occurred in the Barcelona Basin). Calculated erosion of the Litoral and Prelitoral ranges amounted to 1.6 to 2.3 km (Figure 7) and had two effects: (1) it contributed to flexural uplift (erosional rebound); and (2) it reduced topography to a final elevation of 0.3–0.8 km (Figure 7). Erosion of the Litoral Range caused degradation and retreat of the escarpment [e.g., *Kooi and Beaumont*, 1994]. Nevertheless, as the horizontal motion imposed in the Vallès-Penedès hanging wall also involved the Barcelona half-graben, the apparent position of the Prelitoral topographic maximum did not migrate away from the sea.

[50] Our model correctly reproduces the NW-tilted bedding and truncation of the Ebro deposits, with younger strata outcropping in the basin center than along its SE margin, and the topographic profile that presents this sedimentary package as more elevated than its source area (Prelitoral Range; Figure 6, top panel). This particular configuration is a consequence of the interaction between flexural uplift and surface mass transport in the proximal Ebro Basin. As extension progresses, flexural uplift (up to

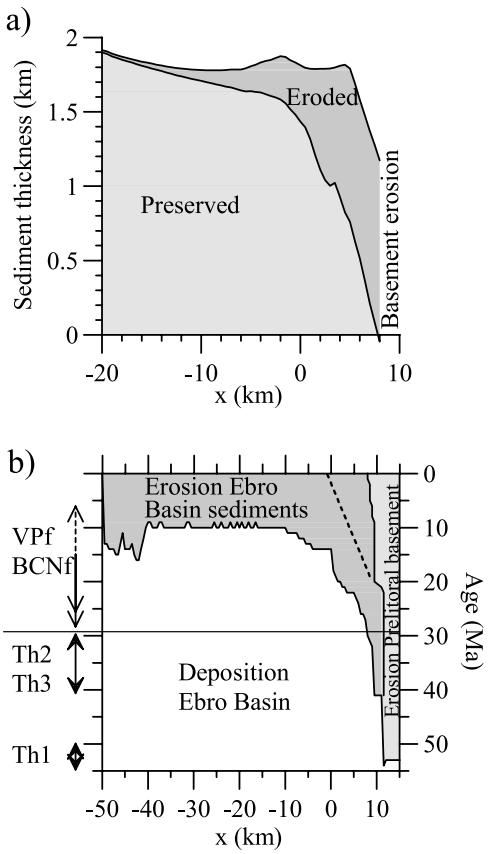

Figure 9. (a) Amount of proximal Ebro Basin deposits eroded from the beginning of erosion until present day. The upper curve denotes the maximum amount of sediments deposited in the Ebro Basin, and the lower curve the amount of sediments remaining in the Ebro Basin after subsequent erosion. Thus the dark shaded area gives the amount of sediments eroded in the Ebro Basin. The onset of this erosion (see Figure 9b) migrated from the CCR toward the centre of the Ebro Basin. (b) Depositional or erosional character of the proximal Ebro Basin through time. Solid line marks the transition between both of them. White area, Ebro Basin deposition; light shading, erosion of Ebro Basin deposits; dark shading, erosion of basement rocks of the Prelitoral Range. Dashed line represents the location of the relative topographic maximum in the Prelitoral Range and proximal Ebro Basin. Arrows denote fault activity periods (same notation as in Table 1).

0.6 km) gradually affects more distal areas of the Ebro Basin (Figure 9b), and consequently the location of the topographic high (sediment source) and the areas subjected to erosion shifts toward the center of the Ebro Basin. The final result of this competition between uplift and erosion is that at the end of the extensional phase erosion prevailed in the most proximal Ebro Basin (<12 km distance from the Prelitoral Range), whereas uplift dominated in its more distal parts. Accordingly during the extensional stage, the topography of the Ebro Basin was reduced by ~0.7 km in its most proximal parts and increased by ~0.7 km in its more distal parts.

5. Discussion

5.1. Lithospheric Rigidity Variations Across the CCR

[51] Our model does not consider lithospheric rigidity changes with time. This assumption is consistent with the relative quiescence of the Ebro Basin area during the Cenozoic [*Riba et al.*, 1983]. However, it is not compatible with the evolution of the SE part of the section (x > 30 km), where lithospheric rigidity was significantly reduced during the Neogene stretching in the Valencia Trough [e.g., *Gaspar-Escribano et al.*, 2003]. The low T_e value adopted in this work for the SE part of the transect, coherent with its Neogene evolution, implies an overestimation of the flexural vertical movements and an increase of deposition in the piggyback basin during the Paleogene (x = 42 km in Figure 7). The T_e distribution used in this paper for the CCR must be regarded as an equivalent value representative for its entire evolution.

[52] The relatively high T_e value (25 km) obtained for the eastern Ebro Basin is consistent with estimates of previous large-scale flexural modeling studies [*Zoetemeijer et al.*, 1990; *Millán et al.*, 1995]. Lower T_e values (as those obtained by *Waltham et al.* [2000] to model short-wavelength features of a small area within the Ebro Basin) would dramatically enhance its flexural rebound during the extensional phase. This would imply complete erosion of the proximal Ebro Basin fill and part of the underlying, undeformed basement, which is contradicted by observations.

[53] Intermediate T_e values (15 km in average) derived for the CCR area correspond to a transitional lithosphere between the relatively strong and weak Ebro Basin and Valencia Trough lithospheres, respectively, and are consistent with a rigidity scenario in which the lithospheric strength of the prerift CCR is concentrated at midcrustal levels [*Gaspar-Escribano et al.*, 2003].

5.2. Timing and Geometry of Faults

[54] Incorporation of thrust Th3 in our model was inspired by the necessity of obtaining a mountainous chain that is wider than the one generated by a two-thrust configuration [*López-Blanco*, 2002]. Such hypothesis is supported by the absence of large values of Eocene sediments [*Roca et al.*, 1999; *Parcerisa*, 2002] and the low amounts of Eocene exhumation [*Gaspar-Escribano*, 2003; *Juez-Larré*, 2003] in the hinterland of the CIC. However, the choice of a more realistic fault transport model than the vertical shear approach used here (such as the kink model [*Suppe*, 1983]), would produce a similar enlargement of the uplifted area. Thus the incorporation of thrust Th3 in the model is not fundamental to explain the Paleogene evolution of the area. Nevertheless, the presence of deformed Triassic and Oligocene sediments in the Barcelona Plain points to intense Paleogene tectonism [*Parcerisa*, 2002] and suggests that such a thrust was actually active and had more importance than previously acknowledged. Similarly to the Vallès-Penedès, the Barcelona fault system probably repre-

sents another major weakness zone [see also *Roca and Guimerà*, 1992] and our modeling results suggest that both Th3 and the SE Collserola fault (Figure 1b) form part of it.

[55] In our model, Paleogene compression involved the activation of two principal thrusts, and thus neglected the development of folds that may have accommodated up to 1.8 km of shortening (Figure 3) [*López-Blanco et al.*, 2000]. Introduction of folding in the model would probably produce a more continuous evolution from 48 to 42 Ma on the three components contributing to topography (Figure 7). However, this would affect the total magnitudes of vertical motions by less than 20%.

[56] The model satisfactorily reproduced geometries of key horizons of the present-day section (topography, bathymetry and base of Tertiary deposits; Figure 6). Minor misfits, such as the too strongly elevated margins of the Litoral Range (preventing the formation of the Barcelona Plain) and of the marginal high SE of the Barcelona graben, could probably be avoided by incorporating in the model secondary faults in the margins of the grabens as well as a kink-like model for fault-block transport. However, this would introduce more complexities (i.e., number of parameters) in our model, obscuring the interpretation of the results.

5.3. Evolution of Vertical Motions

5.3.1. Compressional Stage

[57] Our modeling results are successful in providing a process-based, quantitative explanation for the evolution of vertical motions derived from previous multidisciplinary studies on the tectonic inversion of the CCR. Calculated pale elevations of the CIC of around 1.2–1.9 km at the end of the compressional phase (Figure 7) are in accordance with those derived from petrological and sedimentary studies (0.7–1.2 km mean altitude of the catchment area for Eocene and Late Oligocene fans according to *López-Blanco* [2002] and *Parcerisa* [2002]) and with previous modeling studies [*Garcia-Castellanos et al.*, 2003].

[58] The model predicts Paleogene erosion of 0.8 to 1.3 km of the CIC (Figure 7; x = 12 and 42 km), in agreement with estimates of 0.8–1 km by *López-Blanco et al.* [2000]. This total amount is also compatible with AFT data (Figure 2). However, it appears that AFT and predicted exhumation trends differ on the timing of the main pulse of exhumation, occurring about 8 Myr later in the model. This suggests that the folding phase that occurred during the Lutetian (48–42 Ma) and that was excluded in the model already generated significant topography and erosion. Nevertheless, the lack of resolution of the AFT measurement impedes us be conclusive on this point.

[59] Concerning the proximal Ebro Basin, maximum burial depths of Bartonian (~39 Ma) sediments of 0.8 to 1 km calculated in our model (Figure 7; x = 2 km) agree with results from vitrinite reflectance studies (0.7–0.85 km [*Waltham et al.*, 2000]). As the evolution of the central Ebro Basin is outside the scope of this work, our model does not include its drainage evolution (including the Oligocene-Miocene base level rise) nor the gradual loading effect related to the Pyrenean orogen, which is incorporated as an instantaneous load at the initial stage. This, together with the omission of gradual sediment compaction, explains the systematic underestimate of the calculated subsidence and sedimentation rates in the proximal Ebro Basin (~110 m/Myr) as compared to other studies: ~250 m/Myr for Eocene sediments [*López-Blanco*, 2002] and ~140 m/Myr for Oligocene sediments [*Barberà et al.*, 2001].

[60] Our modeling approach provides time and space continuity to the Late Paleogene history of the proximal Ebro Basin (Figure 9), which is missing in the sedimentary record. An as much as a 1.8 km-thick sedimentary package was deposited along the easternmost margin of the Ebro Basin from Ypresian (~55 Ma) onward (Figure 9a). After deposition, part of this sedimentary cover (up to 1.2 km near the Prelitoral Range) was eroded. This erosional phase commenced in Early Oligocene times (~32 Ma) in the areas closest to the CCR and in Late Miocene times in more distal domains (Figure 9b).

5.3.2. Extensional Stage

[61] The age of the marine-continental transitions in the Barcelona and Vallès-Penedès half-grabens provides paleotopographic constraints for the model. In the Barcelona Basin, this transition is predicted at 24 Ma by our model, in reasonably good agreement with observations (~22 Ma [*Roca et al.*, 1999]). The Late Burdigalian-Langhian (~16 Ma) marine transgression in the Vallès-Penedès Basin [*Cabrera and Calvet*, 1996] occurs with some delay in our model (in Tortonian; ~9 Ma) because the basin is still too elevated. An earlier activation or a more complicated timing of extension along the Vallès-Penedès master fault than the one used in our model (based on the work of *Bartrina et al.* [1992]), could reduce this misfit.

[62] Total Neogene erosion estimates between 1.6 and 2.3 km calculated in our model are in accordance with results of a tectonothermal modeling study (Figure 2) [*Gaspar-Escribano*, 2003] constrained with AFT data [*Juez-Larré*, 2003]. Amounts of sediments deposited in these basins fit reasonably well with present-day basin fill geometries (Figure 6). As the model does not incorporate gradual sediment compaction but considers a constant, average sediment density, the predicted subsidence evolution must be regarded as approximate. In our model, the evolution of basement depth is compared with the total basement subsidence obtained from independent well backstripping studies (Figure 10) [*Bartrina et al.*, 1992]. Modeled and backstripped basement subsidence curves for the Barcelona Basin given in Figure 10 present similar trends, including a phase of subsidence deceleration during Middle Miocene (15–10 Ma). In Figure 10 a subsidence curve is also given for the Vallès-Penedès Basin, in which the poor dating of the mostly continental infill impedes performing a detailed subsidence analysis. For this area, our model predicts that the basement of the Vallès-Penedès Basin subsided at higher rate in the early stages of the extension (25–20 Ma), and that sediment accumulation started only during the Aquitanian (~22 Ma).

[63] Because of the lower prerift topography and the faster subsidence (i.e., larger fault-related tectonic subsidence) of the Barcelona graben with respect to the Vallès-

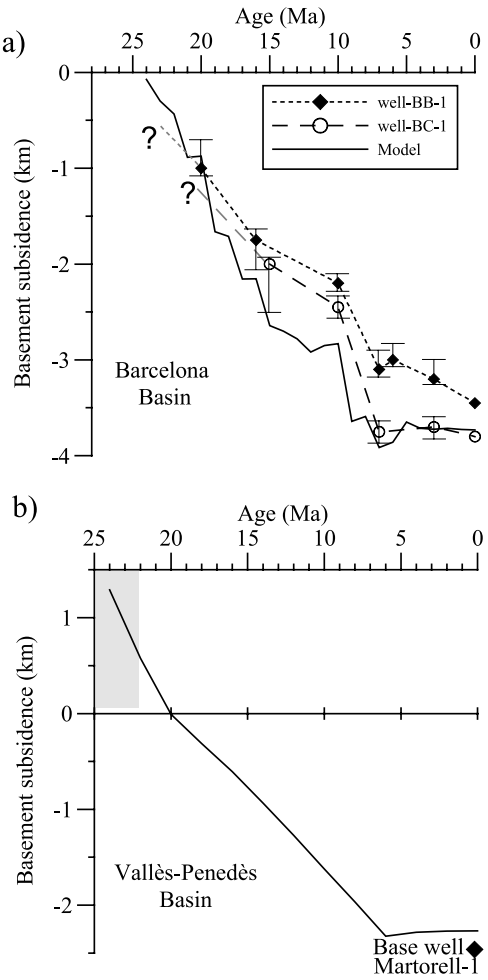

Figure 10. Total basement subsidence predicted by Model 5F. (a) Barcelona Basin. Long-dashed and short-dashed lines with error bars correspond to backstripped wells Barcelona-B1 (B-B1) and Barcelona-C1 (B-C1), respectively [after *Bartrina et al.*, 1992], and thick solid line corresponds to model output (x = 59 km). (b) Vallès-Penedès Basin. The shaded period is nondepositional. Solid diamond corresponds to the pre-Neogene basement depth in the Martorell-1 well [*Bartrina et al.*, 1992].

Penedès Basin, greater accommodation space was created in the Barcelona Basin between 28 and 16 Ma, facilitating an earlier marine transgression. As the Barcelona fault decelerated at 15 Ma (i.e., fault-related tectonic subsidence drastically decreased), flexural uplift diminished and the basin was steadily infilled. By contrast, strong fault-related tectonic subsidence persisted in the Vallès-Penedès Basin after 15 Ma in order to create more accommodation space.

5.4. Neogene Migration of Topographic Maximum

[64] The model proposed in this paper provides a quantitative, self-consistent explanation for the topography of the CCR in terms of interplay between surface transport and flexural uplift, as previously suggested by other authors [e.g., *Anadón et al.*, 1989; *Lewis et al.*, 2000]. In addition, our work confers a primary role to fault tectonics during this interplay, as it controls the location and magnitude of the flexural rebound and topography.

[65] According to our modeling results, the topographic maximum migrated at a constant rate of 0.5 km/Myr during the advancement of the erosional domain toward the Ebro Basin and accelerated from a rate of 0.5 to a rate of 1.5 km/Myr around 15 Ma (Figure 9b and section 4.3.2). This acceleration was ultimately the result of the slip rate reduction on the Barcelona fault at 15 Ma (Table 1), which implied a decrease of the amount of flexural uplift in its footwall (and particularly in the proximal Ebro Basin, Figure 8). Consequently, erosion started to dominate over isostatic uplift in the balance of vertical motions. The larger topographic gradient between the Vallès-Penedès Basin and the Prelitoral Range with respect to the topographic gradient between the Prelitoral Range and the Ebro Basin favored by this time (and not before) this process [see also *Gilchrist and Summerfield*, 1990].

[66] Although fault tectonic forcing was still active until 6 Ma, flexural uplift did not enhance topographic gradients nor did it create extra accumulation space in the proximal Ebro Basin after 9 Ma. Thus, from ~9 Ma onward, no deposition is predicted in the Ebro Basin (Figure 9b). This modeling result is in agreement with previous studies on the evolution of the Ebro Basin [*Riba et al.*, 1983; *Garcia-Castellanos et al.*, 2003] that date the onset of generalized erosion in the Ebro Basin as Middle-Late Miocene. These studies relate this major change to the headwater expansion of the Ebro fluvial network and a sudden base-level drop related to the extension along the southeastern margin of the basin. Our study suggests that, in addition to the Ebro River network development, to the lack of subsidence and unavailability of sediment sources contributed from ~9 Ma onward to nondeposition along the eastern margin of the Ebro Basin.

6. Conclusion

[67] Our study evidences the strong interrelation between fault tectonics, isostasy and surface mass transport by erosion and sedimentation, showing the coupling between processes operating at different scales (from the lithosphere to the surface).

[68] Modeling results concerning the lithospheric framework indicate that relatively high T_e values in the Ebro Basin (T_e = 25 km), gradually changing to low T_e values in the Valencia Trough (T_e = 5 km) are necessary to satisfactorily reproduce present-day basin and fault-block geometries compatible with erosion-deposition patterns in the CCR and proximal Ebro Basin.

[69] In our study area the effect of isostasy and sedimentation/erosion on creation/destruction of topography is nearly in the same range as the effect of thrusting/normal faulting. Thus analyses of the evolution of vertical motions must take into consideration all these processes. In this respect, our model shows that during the Paleogene compressional phase fault-related tectonic uplift of ~3.8 km is partially compensated by erosion of ~1.3 km and isostatic subsidence (up to

1.2 km), resulting in a 1.2–1.9 km high mountain chain at 29 Ma. Moreover, the model shows that during the Chattian-Tortonian (28–7 Ma) extensional phase: (1) The isostatic rebound in the Vallès-Penedès footwall block was mainly influenced by extension along the Barcelona fault (and to a minor degree along the Vallès-Penedès fault). (2) Fault-related tectonic subsidence dominated over flexural uplift and led to the subsidence of the Vallès-Penedès Basin, first by lowering topography and later by creating accommodation space for sediment deposition under essentially continental environments. (3) Large accommodation space in the Barcelona Basin generated by fault-related tectonic subsidence was created during the fast normal motion of the Barcelona fault (28–16 Ma). Subsequently, little tectonic subsidence occurred and marine sediments infilled the basin. (4) During the extensional stage, the location of the topographic maximum shifted from the Prelitoral Range toward the Ebro Basin due to the interaction between flexural uplift and surface mass transport (deposition and erosion). This process accelerated in the Middle Miocene (~15 Ma) while at the same time the velocity of movement along the Barcelona fault and associated footwall flexural uplift decreased.

[70] Our study shows the importance of combining geological data with numerical methods to cover those areas and periods for which data availability is limited and to provide quantitative estimates on geological processes. In this line, we have been capable to constrain the paleoelevation of the Catalan Intraplate Chain during the transition from compression to extension (~29 Ma) to 1.2 to 1.9 km. This result implies a minimum estimate of 15.5 km for the total extension in the Catalan margin during Late Oligocene-Miocene, divided into 10.8 km for the Barcelona fault and 4.7 km for the Vallès-Penedès fault. The model also provides estimates of erosion compatible with thermochronological and other geological data. Total erosion of the CIC during Paleogene was ~1.2 km, and erosion of the CCR during Neogene amounted to 1.9–2.5 km. Along the eastern margin of the Ebro Basin, up to 1.8 km of sediments were deposited during the Paleogene and the Miocene. Subsequently, a large fraction of these sediments (up to 1.2 km) was eroded.

[71] **Acknowledgments.** This paper is publication number 2003.09.04 of the Netherlands Research School of Sedimentary Geology (NSG) and it has been financed by (1) The Earth and Life Sciences (ALW) Council of the Netherlands Organization for Scientific Research (NWO); (2) the project REN2001-1734-C03-03/MAR of the Spanish Science and Technology Ministry (MCYT); and (3) the Research Group of Geodynamics and Basin Analysis (2001SGR00074) from the Generalitat de Catalunya.

References

Abbott, L. D., E. A. Silver, R. S. Anderson, R. Smith, J. C. Ingle, S. A. Kling, D. Haig, E. Small, J. Galewsky, and W. Sliter (1997), Measurement of tectonic surface uplift rate in a young collisional mountain belt, *Nature*, *385*, 501–507.

Anadón, P., L. Cabrera, B. Colldeforns, and A. Sáez (1989), Los sistemas lacustres del Eoceno superior y Oligoceno del sector oriental de la Cuenca del Ebro, *Acta Geol. Hisp.*, *24*, 205–230.

Ayala, C., J. Pous, and M. Torné (1996), The lithosphere-astenosphere boundary of the Valencia Trough (western Mediterranean) deduced from 2D geoid and gravity modelling, *Geophys. Res. Lett.*, *23*, 3131–3134.

Barberà, X., L. Cabrera, M. Marzo, J. M. Parés, and J. Agustí (2001), A complete terrestrial Oligocene magnetobiostratigraphy from the Ebro Basin, *Spain, Earth Planet. Sci. Lett.*, *187*, 1–16.

Bartrina, M. T., L. Cabrera, M. J. Jurado, J. Guimerá, and E. Roca (1992), Evolution of the central Catalan margin of the Valencia Trough (western Mediterranean), *Tectonophysics*, *203*, 219–247.

Cabrera, L., and F. Calvet (1996), Onshore Neogene record in NE Spain: Vallès-Penedès and El Camp half-grabens (NW Mediterranean), in *Tertiary Basins of Spain*, edited by P. F. Friend and C. J. Dabrio, pp. 97–105, Cambridge Univ. Press, New York.

Clauzon, G., J. P. Suc, F. Gautier, A. Berger, and M. F. Loutre (1996), Alternate interpretation of the Messinian salinity crisis: Controversy resolved?, *Geology*, *24*, 363–366.

Coney, P. J., J. A. Muñoz, K. R. McKlay, and C. A. Evenchick (1996), Syntectonic burial and post-tectonic exhumation of the southern Pyrenees foreland fold-thrust belt, *J. Geol. Soc. London*, *153*, 9–16.

Flemings, P. B., and T. E. Jordan (1989), A synthetic stratigraphic model of foreland basins development, *J. Geophys. Res.*, *94*, 3851–3866.

Fontboté, J. M. (1954), Las relaciones tectónicas de la depresión del Vallés-Penedés con la Cordillera Prelitoral Catalana y con la depresión del Ebro, in *Tomo Homenaje Profesor E. Hernández-Pacheco*, pp. 281–310, R. Soc. Esp. Hist. Nat., Madrid.

Gallart, J., N. Vidal, and J. J. Dañobeitia (1994), Lateral variations in deep crustal structure at the Iberian margin of the Valencia trough imaged from seismic reflection methods, *Tectonophysics*, *232*, 59–75.

Garcia-Castellanos, D. (2002), Interplay between lithospheric flexure and river transport in foreland basins, *Basin Res.*, *14*, 89–104.

Garcia-Castellanos, D., M. Fernàndez, and M. Torné (1997), Numerical modeling of foreland basin formation: A program relating thrusting, flexure, sediment geometry and lithophere rheology, *Comput. Geosci.*, *23*, 993–1007.

Garcia-Castellanos, D., M. Fernàndez, and M. Torné (2002), Modelling the evolution of the Guadalquivir foreland basin (south Spain), *Tectonics*, *21*(3), 1018, doi:10.1029/2001TC001339.

Garcia-Castellanos, D., J. Vergés, J. M. Gaspar-Escribano, and S. Cloetingh (2003), Interplay between tectonics, climate and fluvial transport during the Cenozoic evolution of the Ebro Basin (NE Iberia), *J. Geophys. Res.*, *108*(B7), 2347, doi:10.1029/2002JB002073.

Gaspar-Escribano, J. M. (2003), Tectonic modeling of the Catalan Coastal Ranges (NE Spain) and adjacent areas, Ph.D. thesis, 140 pp., Vrije Univ. Amsterdam.

Gaspar-Escribano, J. M., J. D. van Wees, M. ter, Voorde, S. Cloetingh, E. Roca, L. Cabrera, J. A. Muñoz, P. A. Ziegler, and D. García-Castellanos (2001), 3D flexural modeling of the Ebro Basin (NE Iberia), *Geophys. J. Int.*, *145*, 349–367.

Gaspar-Escribano, J. M., M. ter, Voorde, E. Roca, and S. Cloetingh (2003), Mechanical (de)coupling of the lithosphere in the Valencia Trough (NW Mediterranean): What does it mean?, *Earth Planet. Sci. Lett.*, *210*, 291–303.

Gibbs, A. D. (1983), Balanced cross-section construction from seismic sections in areas of extensional tectonics, *J. Struct. Geol.*, *5*, 153–160.

Gilchrist, A. R., and M. A. Summerfield (1990), Differential denudation and flexural isostasy in formation of rifted-margins upwards, *Nature*, *346*, 739–742.

Gómez, M., and J. Guimerà (1999), Estructura alpina de la Serra de Miramar y del NE de las Muntanyes de Prades (Cadana Costero Catalana), *Rev. Soc. Geol. Esp.*, *12*, 405–418.

Guimerà, J. (1984), Paleogene evolution of deformation in the northeastern Iberian Peninsula, *Geol. Mag.*, *121*, 413–420.

Haq, B. U., J. Hardenbol, and P. R. Vail (1987), Chronology of fluctuating sea levels since the Triassic, *Science*, *235*, 1156–1167.

Hossack, J. R. (1979), The use of balanced cross-sections in the calculations of orogenic contractions: A review, *J. Geol. Soc. London*, *136*, 705–711.

Jones, M. A. (1997), Interaction between proximal foreland basin sedimentation and the structural evolution of the Catalan Coastal Range near Gandesa, Catalunya, Spain, Ph.D. thesis, 237 pp., Univ. of Wyo., Laramie.

Juez-Larré, J. (2003), Post Late Paleozoic tectonothermal evolution of the northeast margin of Iberia, assessed by fission-track and (U-Th)/He analysis, Ph.D. thesis, Vrije Univ., Amsterdam.

Lanaja, J. M. (1987), *Contribución de la Exploración Petrolífera al Conocimiento de la Geología de España*, 465 pp., Inst. Geol. y Minero de Esp., Madrid.

Lewis, C. J., J. Vergés, and M. Marzo (2000), High mountains in a zone of extended crust: Insights into the geodynamic development of northeastern Iberia, *Tectonics*, *19*, 86–102.

López-Blanco, M. (2002), Sedimentary response to thrusting and fold growing on the SE margin of the Ebro basin (Paleogene, NE Spain), *Sed. Geol.*, *146*, 133–154.

López-Blanco, M., M. Marzo, D. W. Burbank, J. Vergés, E. Roca, P. Anadón, and J. Piña (2000), Tectonic and climatic controls on the development of foreland fan deltas: Monserrat and

Sant Llorenç del Münt systems (Middle Eocene, Ebro Basin, NE Spain), *Sed. Geol.*, *138*, 17–39.

Losantos, M., E. Aragonès, X. Berástegui, J. Palau, and C. Puidefabregas (1989), Mapa geològic de Catalunya, scale 1:25,0000, Serv. Geol. de Catalunya, Barcelona, Spain.

Martinell, J. (1988), An overview of the marine Pliocene of NE Spain, *Geol. Mediter.*, *15*, 227–233.

Masana, E. (1994), Neotectonic features of the Catalan Coastal Ranges, northeastern Spain, *Acta Geol. Hisp.*, *29*, 107–121.

Millán, H., T. den Bezemer, J. Vergés, J. A. Muñoz, E. Roca, J. Cirés, R. Zoetemeijer, S. Cloetingh, and C. Puigdefábregas (1995), Palaeo-elevation and effective elastic thickness evolution at mountain ranges: Inferences from flexural modelling in the eastern Pyrenees and Ebro Basin, *Mar. Pet. Geol.*, *12*, 917–928.

Morgan, P., and M. Fernàndez (1992), Neogene vertical movements and constraints on extension in the Catalan Coastal Ranges, Iberian Peninsula, and Valencia Trough, western Mediterranean, *Tectonophysics*, *203*, 185–201.

Negredo, A. M., M. Fernández, M. Torné, and D. Doglioni (1999), Numerical modeling of simultaneous extension and compression: The Valencia trough (western Mediterranean), *Tectonics*, *18*, 361–374.

Olivera, C., T. Susagna, A. Roca, and X. Goula (1992), Seismicity of the Valencia Trough and surrounding areas, *Tectonophysics*, *203*, 99–109.

Parcerisa, D. (2002), Petrologia i diagènesi en sediments de l'Oligocè superior i del Miocè inferior i mitjà de la depressió del Vallès i del Plà de Barcelona, Ph.D. thesis, 288 pp., Univ. Autònoma de Barcelona, Barcelona, Spain.

Puigdefábregas, C., J. A. Muñoz, and M. Marzo (1986), Thrust belt development in the eastern Pyrenees and related depositional sequences in the southern foreland basin, in *Foreland Basins*, edited by P. Allen and P. Homewood, *Spec. Publ. Int. Assoc. Sedimentol.*, *8*, 229–246.

Riba, O., S. Reguant, and J. Villena (1983), Ensayo de síntesis estratigráfica y evolutiva de la cuenca terciaria del Ebro, in *Libro Jubilar J.M. Ríos. Geología de España*, pp. 131–159, Inst. Geol. y Minero de Esp., Madrid.

Roca, E. (1996), La evolución geodinámica de la Cuenca Catalano-Balear y áreas adyacentes desde el Mesozoico hasta la actualidad, *Acta Geol. Hisp.*, *29*, 3–25.

Roca, E., and J. Guimerà (1992), The Neogene structure of the eastern Iberian margin: Structural constraints on the crustal evolution of the Valencia Trough (western Mediterranean), *Tectonophysics*, *203*, 203–218.

Roca, E., M. Sans, L. Cabrera, and M. Marzo (1999), Oligocene to Middle Miocene evolution of the central Catalan margin (northwestern Mediterranean), *Tectonophysics*, *315*, 209–229.

Sàbat, F., E. Roca, J. A. Muñoz, J. Vergés, P. Santanach, M. Sans, E. Masana, A. Estévez, and C. Santisteban (1997), Role of extension and compression in the evolution of the eastern margin of Iberia: The ESCI-Valencia Trough seismic profile, *Rev. Soc. Geol. Esp.*, *8*, 431–448.

Salas, R., and A. Casas (1993), Mesozoic extensional tectonics, stratigraphy and crustal evolution during the Alpine cycle of the eastern Iberian basin, *Tectonophysics*, *228*, 33–55.

Sheffels, B., and M. McNutt (1986), Role of subsurface loads and regional compensation in the isostatic balance of the Transverse Ranges, California: Evidence for intracontinental subduction, *J. Geophys. Res.*, *91*, 6419–6431.

Small, E. E., and R. S. Anderson (1995), Geomorphically driven Late Cenozoic rock uplift in the Sierra Nevada, *California, Science*, *270*, 277–280.

Suppe, J. (1983), Geometry and kinematics of fault-bend folding, *Am. J. Sci.*, *283*, 684–721.

Taberner, C., J. Dinarés-Turell, J. Giménez, and C .Docherty (1999), Basin infill architecture and evolution from magnetostratigraphic cross-basin correlations in the southeastern Pyrenean foreland basin, *Geol. Soc. Am. Bull.*, *111*, 1155–1174.

Tucker, G. E., and R. L. Slingerland (1994), Erosional dynamics, flexural isostasy and long-lived escarpments: A numerical modeling study, *J. Geophys. Res.*, *99*, 12,229–12,243.

Turcotte, D. L., and G. Schubert (2001), *Geodynamics*, 2nd ed., 456 pp., Cambridge Univ. Press, New York.

Vergés, J., H. Millán, E. Roca, J. A. Muñoz, M. Marzo, J. Cirés, T. den Bezemer, R. Zoetemeijer, and S. Cloetingh (1995), Eastern Pyrenees and related foreland basins: Pre-, syn- and post-collisional crustal-scale cross-sections, *Mar. Pet. Geol.*, *12*, 903–915.

Vergés, J., M. Marzo, T. Santaeularia, J. Serra-Kiel, D. W. Burbank, J. A. Muñoz, and J. Giménez-Montsant (1998), Quantified vertical motions and tectonic evolution of the SE Pyrenean foreland basin, in *Cenozoic Foreland Basins of Western Europe*, edited by A. Mascle et al., *Geol. Soc. Spec. Publ.*, *134*, 107–134.

Waltham, D., C. Docherty, and C. Taberner (2000), Decoupled flexure in the south Pyrenean foreland, *J. Geophys. Res.*, *105*, 16,329–16,340.

Watts, A. B., and M. Torné (1992), Subsidence history, crustal structure and thermal evolution of the Valencia Trough: A young extensional basin in the western Mediterranean, *J. Geophys. Res.*, *97*, 20,021–20,041.

Watts, A. B., W. S. McKerrow, and E. Fielding (2000), Lithospheric flexure, uplift and landscape evolution in south-central England, *J. Geol. Soc. London*, *157*, 1169–1177.

Zoetemeijer, R., P. Desegaulx, S. Cloetingh, F. Roure, and I. Moretti (1990), Lithospheric dynamics and tectonic-stratigraphic evolution of the Ebro Basin, *J. Geophys. Res.*, *95*, 2701–2711.

S. Cloetingh and D. Garcia-Castellanos, Faculty of Earth and Life Sciences, Vrije Universiteit, De Boelelaan 1085, 1081 HV, Amsterdam, Netherlands.

J. M. Gaspar-Escribano, Escuela Universitaria de Ingeniería Técnica Topográfica, Universidad Politécnica de Madrid, Autovía de Valencia km. 7, 28031 Madrid, Spain. (jgaspar@euitto.upm.es)

E. Roca, Facultat de Geologia, Universitat de Barcelona, c/Martí Franqués s/n, 08071 Barcelona, Spain.